Supplement

Supplementary Figure S1

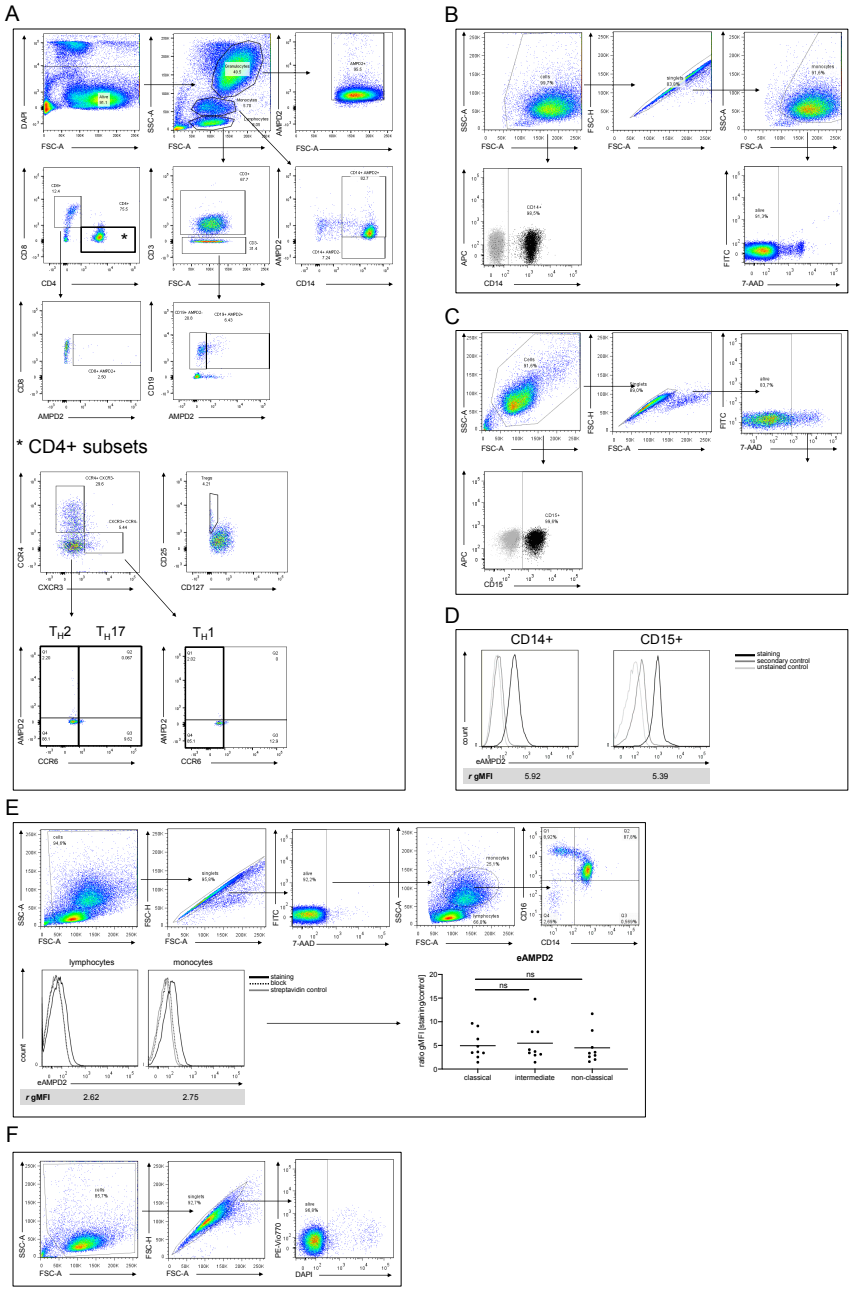

Supplementary Figure S1: (A) Gating strategy. Human leukocytes were isolated by red blood cell lysis. DAPI was used to exclude dead cells. A forward-scatter and side-scatter plot served to identify the different leukocyte subsets. CD4+ T cell subsets were subdivided into Type 1 helper (T_H1) cells, Type 2 helper (T_H2) cells and IL-17-producing T helper (T_H17) cells. T_H1 cells were identified by the expression of CXCR3 in the absence of CCR4 and CCR6. T_H2 cells were defined as CCR4+CXCR3-CCR6-, while T_H17 cells co-expressed CCR4 and CCR6 in the absence of CXCR3. CD4+CD25+CD127low cells were defined as Tregs.[1] Cytotoxic T cells and B cells were identified by the expression of CD8 and CD19, respectively. (B,C) Gating strategy. CD14+ monocytes (B) and CD15+ neutrophil granulocytes (C) were sorted by magnetic cell separation. Purity of > 97% was revealed by surface staining of CD14 and CD15, respectively. Cells were gated using a forward-scatter and side-scatter plot. Doublets were excluded according to the forward-scatter area and height pattern and 7-AAD was used to exclude dead cells. (D) AMPD2 surface expression on CD14+ monocytes and CD15+ neutrophil granulocytes sorted by

magnetic cell separation. The cells were gated according to Supplementary Figures S1B and S1C. *r* gMFI represents the ratio of geometric mean fluorescence intensity of staining to secondary antibody control. (E) PBMCs were gated using a forward-scatter and side-scatter plot. Doublets were excluded according to the forward-scatter area and height pattern and 7-AAD was used to exclude dead cells. *r* gMFI represents the ratio of geometric mean fluorescence intensity of staining to streptavidin control. The staining was successfully blocked by adding 25-fold excess unconjugated antibody. Classical (CD14+ CD16-), intermediate (CD14+ CD16+) and non-classical (CD14- CD16+) monocytes were analyzed individually. The lines on scatter dot plot indicate median. Wilcoxon matched-pairs signed rank test. (F) Gating strategy. Cell lines were gated using a forward-scatter and side-scatter plot. Doublets were excluded according to the forward-scatter area and height pattern and DAPI was used to exclude dead cells.

Supplementary Figure S2

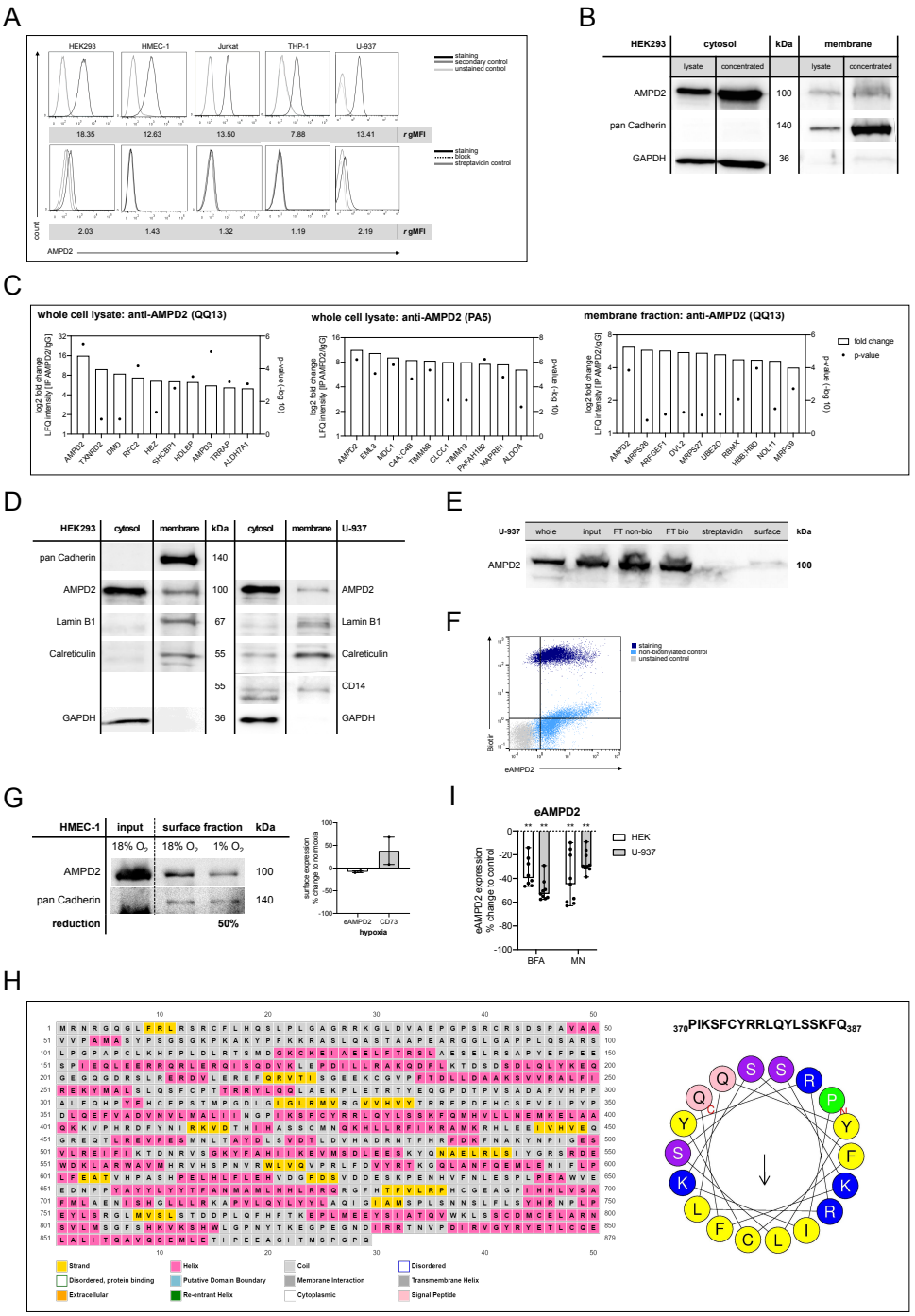

Supplementary Figure S2: (A) Flow cytometric analysis of intracellular (upper row) and surface (lower row) AMPD2 expression in HEK293, HMEC-1, Jurkat, THP-1 and U-937 cell lines. *r* gMFI represents the ratio of geometric mean fluorescence intensity of staining to secondary antibody control and staining to streptavidin control for intracellular and surface stainings, respectively. The surface staining was successfully blocked by adding 25-fold excess unconjugated antibody. (B) Western blot analysis of HEK293 cytosolic and membrane fractions. The samples on the right were concentrated with the help of centrifugal filters to increase to amount of protein analyzed by SDS-PAGE. AMPD2 was detected by the mouse monoclonal anti-AMPD2 antibody clone QQ13. Purity of cytosolic and membrane fractions was verified by analyzing pan Cadherin and GAPDH. Uncropped images are provided in Supplementary Figure S7. (C) Top 10 proteins enriched by IP from HEK293 whole cell lysates and membrane fractions using anti-AMPD2 antibodies QQ13 and PA5, respectively, identified by mass spectrometric analyses. Enrichment is depicted as fold change of LFQ intensity compared to isotype control and was evaluated statistically using two-sample Student's t test. (D) Characterization of HEK293 and U-937 cytosolic and membrane fractions by western blot. Uncropped images are provided in Supplementary Figure S7. (E) Western blot analysis of U-937 cells after surface biotinylation. Intact U-937 cells were biotinylated at 4°C and subsequently lyzed and subjected to streptavidin-based enrichment of biotinylated proteins. Whole cell lysates (whole) were generated by adding Laemmli sample buffer. Biotinylated cell lysates (input) and flow-through (FT) samples of protein not captured by the NeutrAvidin beads were analyzed in parallel. "streptavidin" represents a non-biotinylated control sample that was subjected to streptavidin-based pull-down, while the "surface" sample was prepared by pull-down following surface biotinylation. (F) eAMPD2 expression and surface biotinylation of U-937 cells analyzed by flow cytometry. U-937 cells were fixed after surface biotinylation and stained an anti-AMPD2-antibody (PA5) and streptavidin. Non-biotinylated cells were measured in parallel. The gating strategy is depicted in Supplementary Figure S1F. (G) AMPD2 surface expression in HMEC-1 cells is reduced by hypoxia. Western blot analysis of HMEC-1 whole cell lysate and surface protein enriched by surface biotinylation followed by streptavidin-based pull-down. Cells were cultured under normoxic (18% O_2) or hypoxic (1% O_2) conditions for 24 hours. AMPD2 protein expression was semiquantified relative to pan Cadherin by image analysis and reduction by hypoxia is depicted in relation to normoxic control. Uncropped images are provided in Supplementary Figure S7. The bar graphs show surface expression of eAMPD2 and CD73 under hypoxic conditions analyzed by flow cytometry (n=2). Doublets and dead cells were excluded for analysis as shown in Supplementary Figure S1F. The data are depicted as change in *r* gMFI (geometric mean fluorescence intensity of staining to streptavidin control) in relation to samples cultured under normoxic conditions. (H) The secondary protein structure of AMPD2 was analyzed by the PSIPRED server to identify helical areas (highlighted in pink).[2] The graph on the right depicts the lipid-binding helix predicted by the HeliQuest webserver represented as a helical wheel with the hydrophobic face at the bottom.[3] (I) Golgi inhibition by incubation with 1 µg/mL brefeldin A and 0.5 µg/mL monensin, respectively, for 24 hours reduced AMPD2 surface expression in HEK293 and U-937 cells analyzed by flow cytometry (n=8-9). Doublets and dead cells were excluded for analysis as shown in Supplementary Figure S1F. The data are depicted as change in *r* gMFI (geometric mean fluorescence intensity of staining to secondary antibody control) in relation to untreated control samples.
Bar graphs depict median and range. **p<0.01, compared to untreated control; Wilcoxon matched-pairs signed rank test.
BFA, brefeldin A; MN, monensin

Supplementary Figure S3

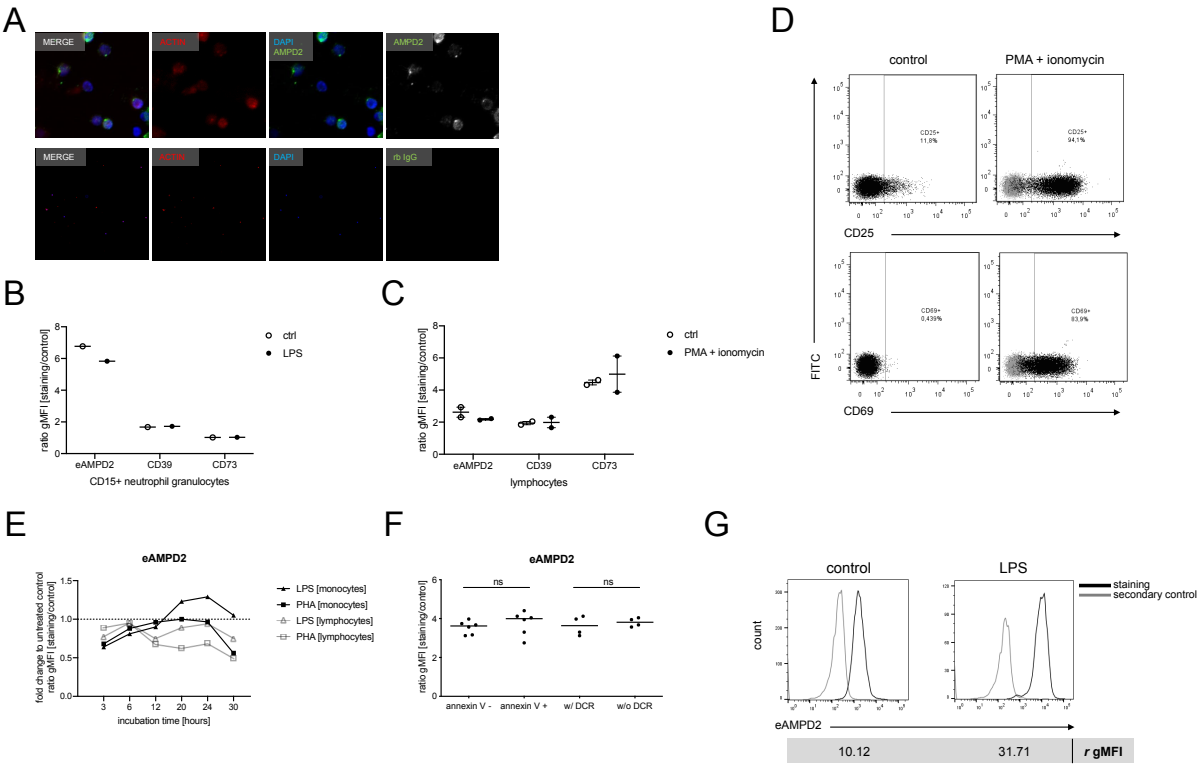

Supplementary Figure S3: (A) Localization of AMPD2 on the cell surface of PBMCs identified by immunofluorescence microscopy. Cells were stained for AMPD2 (green), actin (red) and DAPI (blue). Polyclonal rabbit IgG served as isotype control for the AMPD2 staining antibody. (B) AMPD2 surface expression on CD15+ neutrophil granulocytes sorted by magnetic cell separation. Cells were incubated for 24 hours with 1 µg/mL LPS and expression of eAMPD2, CD39 and CD73 was measured by flow cytometry (n=1). The gating strategy from Supplementary Figure S1C was applied. *r* gMFI represents the ratio of geometric mean fluorescence intensity of staining to secondary antibody control. (C) AMPD2 surface expression on lymphocytes following stimulation. PBMCs were treated with 10 ng/mL PMA + 1 µg/mL ionomycin for 24 hours and expression of eAMPD2, CD39 and CD73 was measured by flow cytometry (n=2). Lymphocytes were gated according to Supplementary Figure S1E for analysis. *r* gMFI represents the ratio of geometric mean fluorescence intensity of staining to secondary antibody control. (D) Proof of lymphocyte activation. Expression of CD25 and CD69 was measured by flow cytometry after 24-hour stimulation with 10 ng/mL PMA + 1 µg/mL ionomycin compared to untreated control. Cells were incubated in PBMC co-culture and lymphocytes were gated according to Supplementary Figure S1E for analysis. (E) Kinetics of AMPD2 surface expression in human PBMC co-culture after incubation with 1 µg/mL LPS or 5 µg/mL PHA determined by flow cytometric analysis. The gating strategy from Supplementary Figure S1E was applied. Data are expressed as mean (n=2) ratio to untreated control. (F) The effect of apoptosis on eAMPD2 staining on human monocytes from PBMC co-culture treated with LPS. Apoptotic cells were identified with the help of annexin V. The gating strategy is depicted in Supplementary Figure S1E. In the right-hand approach apoptotic cells were removed by dead cell removal (DCR) after incubation. Apoptosis does not significantly influence AMPD2 surface expression. (G) AMPD2 surface staining on primary human monocytes analyzed by flow cytometry. PBMCs were incubated for 24 hours with or without 1 µg/mL LPS. Monocytes were gated according to Supplementary Figure S1E for analysis. *r* gMFI represents the ratio of geometric mean fluorescence intensity of staining to secondary antibody control.

Box plots show median and range. The lines on scatter dot plot indicate median. Wilcoxon matched-pairs signed rank test.

Supplementary Figure S4

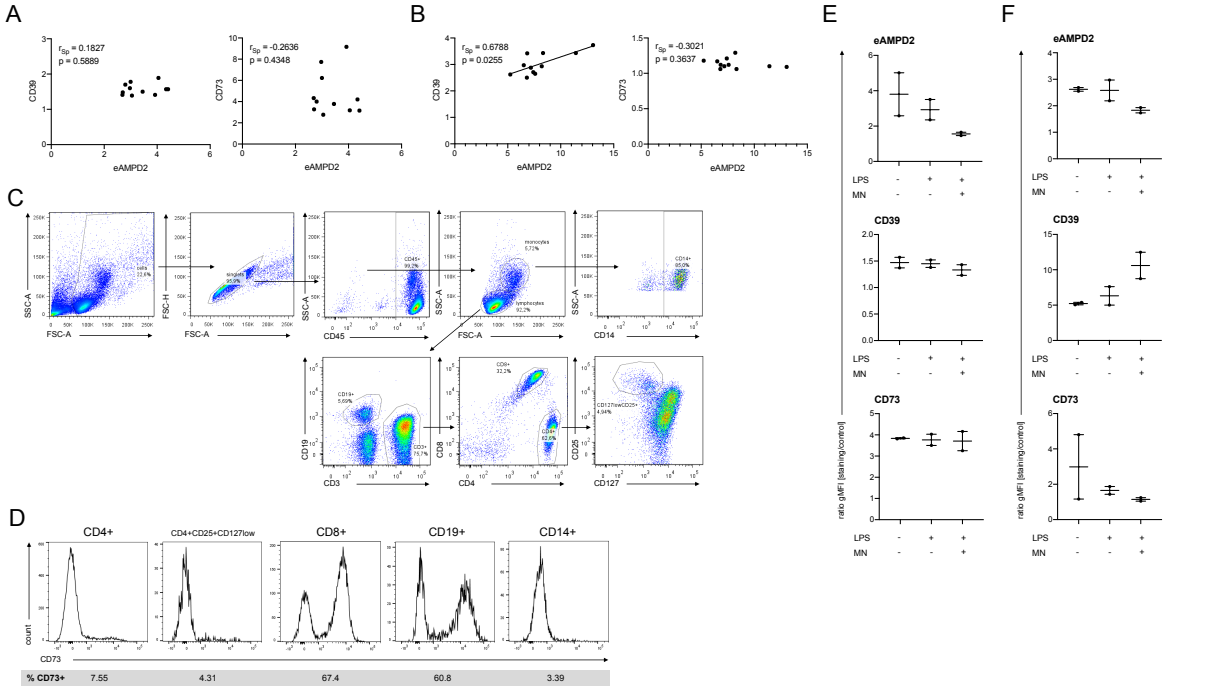

Supplementary Figure S4: Flow cytometric analysis of eAMPD2, CD39 and CD73 expression on primary human immune cell populations at baseline. Correlation between eAMPD2 and ectonucleotidase expression in (A) lymphocytes and (B) monocytes from healthy donors after PBMC isolation. eAMPD2, CD39 and CD73 expression was determined by flow cytometry. The gating strategy from Supplementary Figure S1E was applied. Expression is depicted as ratio of geometric mean fluorescence intensity of staining to secondary antibody control. eAMPD2 correlates with CD39 surface expression in monocytes. Spearman's Rank-Order Correlation. (C) PBMCs were gated using a forward-scatter and side-scatter plot. Doublets were excluded according to the forward-scatter area and height pattern and leukocytes were identified by the expression of CD45. Lymphocytes and monocytes were gated according to their distinctive appearance in a forward-scatter and side-scatter plot. Lymphocytes were subdivided depending on the surface expression of CD4 and CD8. CD4+CD25+CD127low cells were defined as regulatory T cells. CD19+ B cells and CD14+ monocytes were evaluated separately. (D) CD73 surface expression on immune cells subdivided according to Supplementary Figure S4C. (E,F) AMPD2 surface expression on human PBMCs is reduced by Golgi transport inhibition. Cells were treated with 1 µg/mL LPS with or without 0.5 µg/mL monensin (MN) (n=2) for 21-24 hours and surface expression of AMPD2, CD39 and CD73 was measured by flow cytometry. Lymphocytes (E) and monocytes (F) were incubated in co-culture and gated according to Supplementary Figure S1E for analysis. *r* gMFI represents the ratio of geometric mean fluorescence intensity of staining to secondary antibody control.
All boxplots show median and minimum or maximum values, respectively.

Supplementary Figure S5

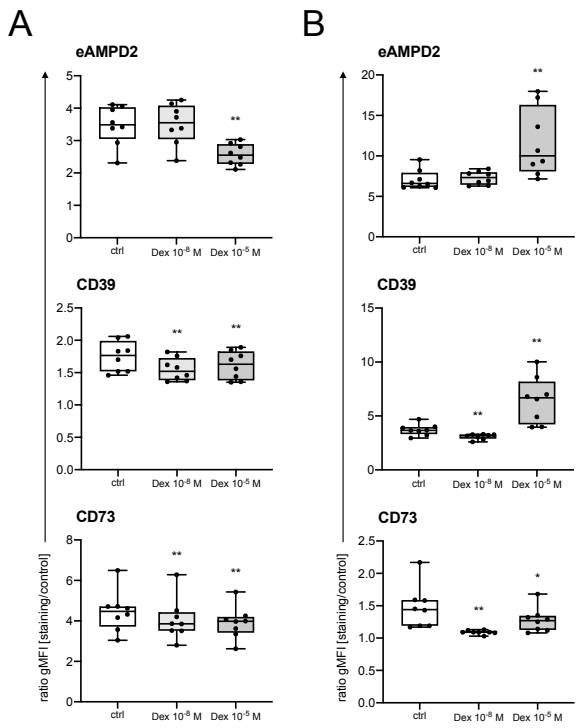

Supplementary Figure S5: AMPD2 surface expression on human PBMCs following immunomodulation. Cells were treated with 10^{-8} M and 10^{-5} dexamethasone, respectively (n=8). Surface expression of eAMPD2, CD39 and CD73 was measured by flow cytometry. (A) Lymphocytes and (B) monocytes were incubated in co-culture and gated according to Supplementary Figure S1E for analysis. All boxplots show median, interquartile range, and minimum or maximum values, respectively. *p<0.05, **p<0.01; Wilcoxon matched-pairs signed rank test.

Supplementary Figure S6

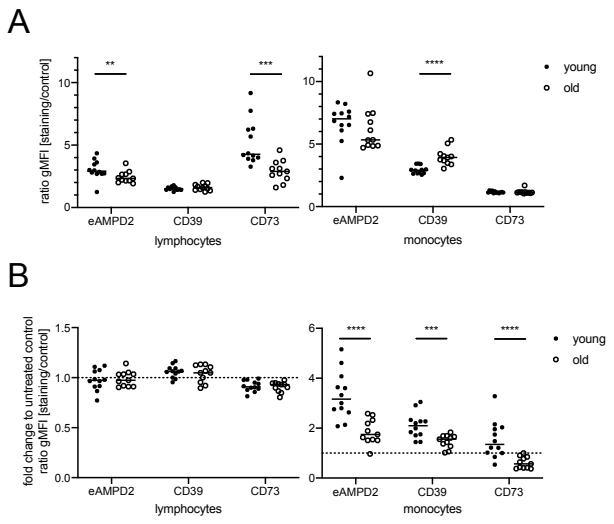

Supplementary Figure S6: eAMPD2, CD39 and CD73 expression depending on donor age. PBMCs were isolated from heparinized blood samples of young (≤40 years) and old (≥50 years) healthy donors. (A) eAMPD2, CD39 and CD73 expression was analyzed by flow cytometry directly after isolation (n=11-12). PBMCs were gated according to Supplementary Figure S1E for analysis. (B) Flow cytometric analysis of eAMPD2, CD39 and CD73 expression after incubation with 1 µg/mL LPS for 21-24 hours in co-culture (n=11-12). PBMCs were gated according to Supplementary Figure S1E for analysis. Modification by LPS stimulation is depicted in relation to untreated control samples.

Lines on scatter dot plot represent median. **p<0.01, ***p<0.001, ****p<0.0001, Mann Whitney test.

Supplementary Figure S7

Supplementary Figure S7: Uncropped western blot images corresponding to (A) Figure 2B, (B) Figure 2C, (C) Supplementary Figure S2E, (D) Figure 2E, (E) Figure 3C, (F) Figure 4F, (G) Supplementary Figure S2B, (H) Supplementary Figure S2D, and (I) Supplementary Figure S2G. (J) Protein standard used for all western blots.

Supplementary Table S1: Mass spectrometric analyses of top 10 proteins immunoprecipitated from HEK293 samples using anti-AMPD2 antibodies

Gene name	Peptides	Unique peptides	Student's t test Difference LFQ intensity	Student's t-test p-value (-log10) LFQ intensity	Median intensity	Intensity rank
total: IP QQ13						
AMPD2	47	1	16,303	5,516	90290000000	1
SHCBP1	3	3	7,703	2,805	338410000	60
RFC2	21	21	7,267	4,166	373610000	54
TXNRD2	11	10	6,774	0,925	3809600000	7
DMD	8	7	6,560	0,931	1460400000	15
HDLBP	81	81	5,936	3,519	18038000	319
HBZ	1	1	5,792	1,342	306520000	66
TRRAP	15	15	5,686	3,199	84882000	163
AMPD3	5	4	5,491	5,041	67224000	191
ALDH7A1	43	43	5,258	3,076	38252000	232
total: IP PA5						
AMPD2	47	1	11,237	6,215	4961800000	5
EML3	24	24	9,992	5,077	1539000000	21
MDC1	35	35	9,269	5,789	790850000	43
CLCC1	22	22	9,144	2,917	1159600000	27
C4A;C4B	7	6	8,266	4,654	452350000	84
TIMM8B	9	9	8,226	5,364	294480000	114
TIMM13	8	8	8,044	2,908	584640000	62
MAPRE1	34	31	7,755	4,784	315370000	106
PAFAH1B2	15	15	7,539	6,233	611770000	59
ALDOA	60	53	7,346	2,374	227920000	136
membrane: IP QQ13						
AMPD2	47	1	5,815	3,849	311700000	34
HBB;HBD	3	2	4,658	3,967	30926000	185
UBE2O	33	33	4,557	1,156	32560000	181
NOL11	22	22	4,392	1,494	18015000	257
MRPS27	27	27	4,349	1,114	81540000	89
ARFGEF1	4	4	4,204	1,158	35380000	164
RBMX	40	15	4,179	2,062	43027000	147
MRPS9	29	29	4,114	2,713	54771000	124
MRPS26	23	23	4,086	0,811	23443000	221
DVL2	8	6	4,041	1,285	45793000	142

IP from HEK293 whole cell lysates (total) and membrane fractions (membrane) was performed using anti-AMPD2 antibodies QQ13 and PA5, respectively. Differential protein abundance compared to isotype control was calculated using two-sample Student's t test.

Supplementary Table S2: Mass spectrometric analysis of surface-enriched protein from HMEC-1 cells

							LFQ: surface enrichment vs. non-biotinylated control	
Protein name	**Gene name**	**Peptides**	**Unique peptides**	**Intensity**	**iBAQ**	**Plasma membrane†**	**p-value (-log10)**	**t test Difference (log2)**
Cell surface glycoprotein MUC18	MCAM	33	33	23992000000	666430000	+	4,0	10,0
CD166 antigen	ALCAM	35	35	57127000000	1680200000	+	6,1	9,3
Poliovirus receptor	PVR	9	9	9538200000	681300000	+	4,5	9,2
Dystroglycan	DAG1	20	20	8242400000	179180000	+	4,2	8,9
Beta-2-microglobulin	B2M	5	2	17015000000	2126800000	+	3,1	8,8
Receptor-type tyrosine-protein phosphatase F	PTPRF	54	51	4795000000	43198000	+	4,0	8,7
Myelin protein zero-like protein 1	MPZL1	10	6	5678400000	516220000	+	5,7	8,4
Vinculin	VCL	72	72	64726000000	752630000	+	3,7	8,4
Non-specific lipid-transfer protein	SCP2	28	28	19103000000	596960000	+	5,6	8,4

AMPD2	
Peptides	23
Unique peptides	23
Sequence coverage [%]	25,4
Unique sequence coverage [%]	25,4
Molecular weight [kDa]	100,69
Q-value	0
Score	30,278
Intensity	978860000
iBAQ	20827000
MS/MS count	64
LFQ: surface enrichment vs. non-biotinylated control	
t test Difference (log2)	3,6998
p-value (-log10)	2,0048
LFQ: surface enrichment vs. input	
t test Difference (log2)	3,1967
p-value (-log10)	4,2404

Top abundant proteins and enrichment of AMPD2 by surface biotinylation. Surface-enriched samples were obtained by surface biotinylation of HMEC-1 cells followed by streptavidin-based pull-down. Differential protein

abundance compared to non-biotinylated samples undergoing streptavidin-based pull-down (non-biotinylated control) and biotinylated whole cell lysate (input) was determined using two-sample Student's t test.
† Plasma membrane annotation according to the Gene Ontology project.[4, 5]

Supplementary Table S3: Search for lipid-binding helices according to the HeliQuest decision tree

Sequence	μH	z	D
116SMDGKCKEIAEELFTRSL135	0,319	-1	-0,028864
118MDGKCKEIAEELFTRSLA136	0,302	-1	-0,044912
120DGKCKEIAEELFTRSLAE137	0,249	-2	-0,424944
121GKCKEIAEELFTRSLAES138	0,284	-1	-0,061904
151SPIEQLEERRQRLERQIS168	0,455	0	0,42952
152PIEQLEERRQRLERQISQ169	0,464	0	0,438016
153IEQLEERRQRLERQISQD170	0,415	-1	0,06176
154EQLEERRQRLERQISQDV171	0,391	-1	0,039104
155QLEERRQRLERQISQDVK172	0,407	1	0,714208
156LEERRQRLERQISQDVKL173	0,378	1	0,686832
157EERRQRLERQISQDVKLE174	0,248	0	0,234112
158ERRQRLERQISQDVKLEP175	0,243	1	0,559392
159RRQRLERQISQDVKLEPD176	0,25	1	0,566
160RQRLERQISQDVKLEPDI177	0,327	0	0,308688
161QRLERQISQDVKLEPDIL178	0,436	-1	0,081584
162RLERQISQDVKLEPDILL179	0,366	-1	0,015504
163LERQISQDVKLEPDILLR180	0,366	-1	0,015504
164ERQISQDVKLEPDILLRA181	0,306	-1	-0,041136
165RQISQDVKLEPDILLRAK182	0,296	1	0,609424
166QISQDVKLEPDILLRAKQ183	0,255	0	0,24072
167ISQDVKLEPDILLRAKQD184	0,264	-1	-0,080784
168SQDVKLEPDILLRAKQDF185	0,264	-1	-0,080784
169QDVKLEPDILLRAKQDFL186	0,282	-1	-0,063792
192SDLQLYKEQGEGQGDRSL209	0,142	-2	-0,525952
193DLQLYKEQGEGQGDRSLR210	0,196	-1	-0,144976
194LQLYKEQGEGQGDRSLRE211	0,197	-1	-0,144032
195QLYKEQGEGQGDRSLRER212	0,072	0	0,067968
196LYKEQGEGQGDRSLRERD213	0,102	-1	-0,233712
197YKEQGEGQGDRSLRERDV214	0,107	-1	-0,228992
234FTDLLDAAKSVVRALFIR251	0,426	1	0,732144
235TDLLDAAKSVVRALFIRE252	0,295	0	0,27848
236DLLDAAKSVVRALFIREK253	0,332	1	0,643408
237LLDAAKSVVRALFIREKY254	0,275	2	0,9196
238LDAAKSVVRALFIREKYM255	0,251	2	0,896944
239DAAKSVVRALFIREKYMA256	0,249	2	0,895056
240AAKSVVRALFIREKYMAL257	0,126	3	1,108944

Sequence	μH	z	D
241AKSVVRALFIREKYMALS258	0,113	3	1,096672
242KSVVRALFIREKYMALSL259	0,172	3	1,152368
243SVVRALFIREKYMALSLQ260	0,148	2	0,799712
244VVRALFIREKYMALSLQS261	0,148	2	0,799712
245VRALFIREKYMALSLQSF262	0,173	2	0,823312
246RALFIREKYMALSLQSFC263	0,181	2	0,830864
247ALFIREKYMALSLQSFCP264	0,097	1	0,421568
361VLMALIINGPIKSFCYRR378	0,099	3	1,083456
362LMALIINGPIKSFCYRRL379	0,077	3	1,062688
363MALIINGPIKSFCYRRLQ380	0,161	3	1,141984
364ALIINGPIKSFCYRRLQY381	0,153	3	1,134432
365LIINGPIKSFCYRRLQYL382	0,219	3	1,196736
366IINGPIKSFCYRRLQYLS383	0,287	3	1,260928
367INGPIKSFCYRRLQYLSS384	0,346	3	1,316624
368NGPIKSFCYRRLQYLSSK385	0,232	4	1,539008
369GPIKSFCYRRLQYLSSKF386	0,338	4	1,639072
370PIKSFCYRRLQYLSSKFQ387	0,346	4	1,646624
371IKSFCYRRLQYLSSKFQM388	0,329	4	1,630576
372KSFCYRRLQYLSSKFQMH389	0,248	4	1,554112
373SFCYRRLQYLSSKFQMHV390	0,319	3	1,291136
374FCYRRLQYLSSKFQMHVL391	0,246	3	1,222224
375CYRRLQYLSSKFQMHVLL392	0,249	3	1,225056
376YRRLQYLSSKFQMHVLLN393	0,156	3	1,137264
377RRLQYLSSKFQMHVLLNE394	0,119	2	0,772336
378RLQYLSSKFQMHVLLNEM395	0,011	1	0,340384
379LQYLSSKFQMHVLLNEMK396	0,012	1	0,341328
380QYLSSKFQMHVLLNEMKE397	0,139	0	0,131216
381YLSSKFQMHVLLNEMKEL398	0,185	0	0,17464
382LSSKFQMHVLLNEMKELA399	0,165	0	0,15576
383SSKFQMHVLLNEMKELAA400	0,239	0	0,225616
515GKYFAHIIKEVMSDLEES532	0,522	-2	-0,167232
516KYFAHIIKEVMSDLEESK533	0,494	-1	0,136336
517YFAHIIKEVMSDLEESKY534	0,392	-2	-0,289952
518FAHIIKEVMSDLEESKYQ535	0,411	-2	-0,272016
550VYRTKGQLANFQEMLENI597	0,436	0	0,411584
551YRTKGQLANFQEMLENIF598	0,455	0	0,42952

Sequence	μH	z	D
582RTKGQLANFQEMLENIFL599	0,419	0	0,395536
583TKGQLANFQEMLENIFLP600	0,396	-1	0,043824
584KGQLANFQEMLENIFLPL601	0,476	-1	0,119344
585GQLANFQEMLENIFLPLF602	0,468	-2	-0,218208
586QLANFQEMLENIFLPLFE603	0,503	-3	-0,515168
587LANFQEMLENIFLPLFEA604	0,511	-3	-0,507616
588ANFQEMLENIFLPLFEAT605	0,441	-3	-0,573696
589NFQEMLENIFLPLFEATV606	0,409	-3	-0,603904
590FQEMLENIFLPLFEATVH607	0,382	-3	-0,629392
591QEMLENIFLPLFEATVHP608	0,332	-3	-0,676592
592EMLENIFLPLFEATVHPA609	0,345	-3	-0,66432
593MLENIFLPLFEATVHPAS610	0,314	-2	-0,363584
594LENIFLPLFEATVHPASH611	0,332	-2	-0,346592
595ENIFLPLFEATVHPASHP612	0,279	-2	-0,396624
596NIFLPLFEATVHPASHPE613	0,279	-2	-0,396624
597IFLPLFEATVHPASHPEL614	0,152	-2	-0,516512
598FLPLFEATVHPASHPELH615	0,148	-2	-0,520288
599LPLFEATVHPASHPELHL616	0,143	-2	-0,525008
600PLFEATVHPASHPELHLF617	0,143	-2	-0,525008
601LFEATVHPASHPELHLFL618	0,09	-2	-0,57504
602FEATVHPASHPELHLFLE619	0,116	-3	-0,880496
603EATVHPASHPELHLFLEH620	0,07	-3	-0,92392
645PEAWVEEDNPPYAYYLYY662	0,2	-4	-1,1312
646EAWVEEDNPPYAYYLYYT663	0,183	-4	-1,147248
647AWVEEDNPPYAYYLYYTF664	0,091	-3	-0,904096
648WVEEDNPPYAYYLYYTFA665	0,091	-3	-0,904096
649VEEDNPPYAYYLYYTFAN666	0,127	-3	-0,870112
650EEDNPPYAYYLYYTFANM667	0,128	-3	-0,869168
651EDNPPYAYYLYYTFANMA668	0,164	-2	-0,505184
652DNPPYAYYLYYTFANMAM669	0,107	-1	-0,228992
653NPPYAYYLYYTFANMAML670	0,054	0	0,050976
654PPYAYYLYYTFANMAMLN671	0,054	0	0,050976
655PYAYYLYYTFANMAMLNH672	0,085	0	0,08024
656YAYYLYYTFANMAMLNHL673	0,095	0	0,08968
657AYYLYYTFANMAMLNHLR674	0,068	1	0,394192
659YYLYYTFANMAMLNHLRR675	0,133	2	0,785552

Sequence	μH	z	D
660YLYYTFANMAMLNHLRRQ676	0,116	2	0,769504
694IHHLVSAFMLAENISHGL711	0,242	-1	-0,101552
695HHLVSAFMLAENISHGLL712	0,24	-1	-0,10344
696HLVSAFMLAENISHGLLL713	0,155	-1	-0,18368
697LVSAFMLAENISHGLLLR714	0,174	0	0,164256
698VSAFMLAENISHGLLLRK715	0,056	1	0,382864
699SAFMLAENISHGLLLRKA716	0,025	1	0,3536
700AFMLAENISHGLLLRKAP717	0,018	1	0,346992
701FMLAENISHGLLLRKAPV718	0,056	1	0,382864
702MLAENISHGLLLRKAPVL719	0,058	1	0,384752
703LAENISHGLLLRKAPVLQ720	0,129	2	0,781776
704AENISHGLLLRKAPVLQY721	0,116	1	0,439504
705ENISHGLLLRKAPVLQYL722	0,19	1	0,50936
706NISHGLLLRKAPVLQYLY723	0,177	2	0,827088
707ISHGLLLRKAPVLQYLYY724	0,091	2	0,745904
708SHGLLLRKAPVLQYLYYL725	0,09	2	0,74496
791SCDMCELARNSVLMSGFS808	0,032	-1	-0,299792
792CDMCELARNSVLMSGFSH809	0,036	-1	-0,296016
793DMCELARNSVLMSGFSHK810	0,118	0	0,111392
794MCELARNSVLMSGFSHKV811	0,158	1	0,479152
795CELARNSVLMSGFSHKVK812	0,126	2	0,778944
796ELARNSVLMSGFSHKVKS813	0,211	2	0,859184
797LARNSVLMSGFSHKVKSH814	0,231	3	1,208064
798ARNSVLMSGFSHKVKSHV815	0,254	3	1,229776
837DIRVGYRYETLCQELALI854	0,166	-1	-0,173296
838IRVGYRYETLCQELALIT855	0,219	0	0,206736
839RVGYRYETLCQELALITQ856	0,291	0	0,274704
840VGYRYETLCQELALITQA857	0,262	-1	-0,082672
841GYRYETLCQELALITQAV858	0,262	-1	-0,082672
842YRYETLCQELALITQAVQ859	0,263	-1	-0,081728
843RYETLCQELALITQAVQS860	0,317	-1	-0,030752
844YETLCQELALITQAVQSE861	0,325	-3	-0,6832
845ETLCQELALITQAVQSEM862	0,338	-3	-0,670928
846TLCQELALITQAVQSEML863	0,262	-2	-0,412672
847LCQELALITQAVQSEMLE864	0,304	-3	-0,703024

Helical domains present in AMPD2 protein sequence as identified by the PSIPRED server (shown in Supplementary Figure 2H) were submitted to the HeliQuest webserver.[2, 3] D was calculated as follows: D = 0.944(<μH>) + 0.33(z). Lipid-binding helix were defined by D > 1.34 (highlighted in green), possible lipid-binding helices were defined by 0.68 < D < 1.34 (highlighted in yellow).
μH, hydrophobic moment; z, net charge; D, discrimination factor

Supplementary Table S4: Mass spectrometric analyses of top 10 proteins immunoprecipitated from CD14+ monocyte samples by anti-AMPD2 antibody (QQ13)

Gene name	Peptides	Unique peptides	Student's t test Difference LFQ intensity	Student's t test p-value (-log 10) LFQ intensity	Intensity
RAB5C	8	6	7,833	3,858	3500500000
PRKAA1	2	2	7,738	2,826	2328900000
LPCAT2	2	2	6,740	4,248	1221300000
GNAI2	13	7	5,932	3,962	1741800000
AMPD2	8	8	4,239	2,869	195980000
SPTBN	2	2	3,969	1,921	131030000
GNPAT	1	1	3,954	2,940	219120000
TRPV2	5	5	3,876	2,898	215710000
IDH2	11	11	3,646	3,273	1720800000
CLIP1	1	1	2,899	0,368	10001000000

CD14+ monocytes were isolated by MACS. IP from membrane fractions was performed using anti-AMPD2 antibody QQ13. Differential protein abundance compared to isotype control was calculated using two-sample Student's t test.

Supplementary Table S5: Characteristics of donors divided into age-related groups

	young	old
donors, n	12	11
age [years], median (IQR)	27 (26-31.75)	61 (55-78)
age [years], range	25-40	50-86
female, n (%)	9 (82)	7 (64)

IQR, interquartile range

References

1. Cossarizza A, Chang HD, Radbruch A, et al. Guidelines for the use of flow cytometry and cell sorting in immunological studies. *European journal of immunology*. Oct 2017;47(10):1584-1797.
2. Jones DT. Protein secondary structure prediction based on position-specific scoring matrices. *J Mol Biol*. Sep 17 1999;292(2):195-202.
3. Gautier R, Douguet D, Antonny B, Drin G. HELIQUEST: a web server to screen sequences with specific alpha-helical properties. *Bioinformatics*. Sep 15 2008;24(18):2101-2.
4. Ashburner M, Ball CA, Blake JA, et al. Gene ontology: tool for the unification of biology. The Gene Ontology Consortium. *Nat Genet*. May 2000;25(1):25-9.
5. The Gene Ontology resource: enriching a GOld mine. *Nucleic acids research*. Jan 8 2021;49(D1):D325-d334.